THE JOURNAL OF PHYSICAL CHEMISTRY B

Article

pubs.acs.org/JPCB

Temperature Influence on the Structure and Interfacial Properties of Surfactin Micelle: A Molecular Dynamics Simulation Study

An-Qi She, Hong-Ze Gang, and Bo-Zhong Mu*

State Key Laboratory of Bioreactor Engineering and Institute of Applied Chemistry, East China University of Science and Technology, Shanghai, P. R. China 200237

Supporting Information

ABSTRACT: Surfactin is an efficient biosurfactant excreted by different strains of *Bacillus subtilis*. Our study provides a molecular view of the temperature dependence of the structure and the interfacial properties of un-ionized surfactin micelles. The overall size and shape, the surface area, the radial density distribution of the micelles, the conformation of the hydrocarbon chain, and the intramolecular/intermolecular hydrogen bonds formed in surfactin molecules were investigated. The micelles were mostly in sphere shapes, and the radii of surfactin micelle were estimated to be around 2.2 nm. The peptide rings occupied most of the surface of the micelles. Small amounts of β-turn and γ-turn structures were found in the conformations of the peptide rings. When the temperature increased, the shape of the peptide rings became planar; the solvent accessible surface area decreased as temperature dehydration occurred. At 343 K some hydrocarbon chains reversed their orientation (flip-flopped). In addition, the stability of the hydrogen bond interactions in the micelles decreases with the increasing temperature.

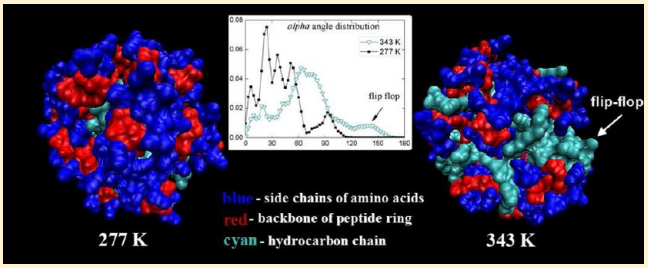

1. INTRODUCTION

Surfactin is a kind of biosurfactant produced by several *Bacillus subtilis* strains.[1] It consists of a heptapeptide bonded to a β-hydroxyl fatty acid and closed via a lactone bond.[2] The peptide moiety of the surfactin molecule was characterized to adopt a "horse-saddle" topology in DMSO solution as a special conformation by Bonmatin et al.[3] Surfactin could reduce the surface tension of water from 72 to 27 mN m^{-1} at a concentration of 1×10^{-5} M.[1,4] Besides, surfactin also exhibits significant biological activities, such as antibacterial,[5] anti-HIV,[6] and antitumor.[7] These surface activities and biological properties are closely related to the conformation and assembly of the surfactin molecules in micelles.

Recently, several experimental investigations[8−10] have been devoted to understanding the structures of the surfactin micelles. The study conducted by Knoblich et al.[8] revealed that surfactin micelles were in both spherical and ellipsoidal shapes at pH 7, whereas the diameters of the spherical micelles were 5−9 nm, and the length and width of the ellipsoidal micelles were approximately 19 and 11 nm, respectively, by cryo-micrographs. Han and co-workers[9] detected that small surfactin aggregates with hydrodynamic radius of 4−6 nm dominated in the micelle solutions by dynamic light scattering (DLS) and transmission electron microscopy (TEM) measurements. Shen et al.[10] found that the aggregation number of surfactin micelle was at 20 ± 5 and the diameter of the micelle was 50 ± 5 Å by means of small-angle neutron scattering (SANS), and the structure of the micelle was of the core−shell type with the hydrocarbon chain and the four hydrophobic leucines forming the core of the micelle.

Nowadays, molecular dynamics (MD) simulations has been massively used to study various kinds of surfactant micelles such as sodium dodecyl sulfate (SDS),[11−16] glycolipid,[17,18] dodecylphosphocholine (DPC),[19−21] and so on. This method provides a complementary view to reveal detailed information that is often very difficult or even impossible to achieve experimentally. As for surfactin micelles, they have rarely been studied by computational methods, though several studies[22−25] have been made for investigating the structures and properties of the surfactin molecule at the hydrophilic/hydrophobic interface by molecular simulation.

In the present study we performed MD simulations of surfactin micelle, which consisted with 25 un-ionized iso-C16 surfactin molecules (16 denotes the carbon number in fatty acid moiety), in aqueous solution separately at four temperatures, namely, 277, 298, 323, and 343 K, in order to explore the influence of ambient temperature on the micelle structure and interfacial properties.

2. METHODS

The chemical composition of the un-ionized iso-C16 surfactin used here is presented in Figure 1. The secondary structure of the peptide ring backbones of iso-C16 surfactin adopted the S1

Received: March 13, 2012
Revised: September 17, 2012
Published: September 22, 2012

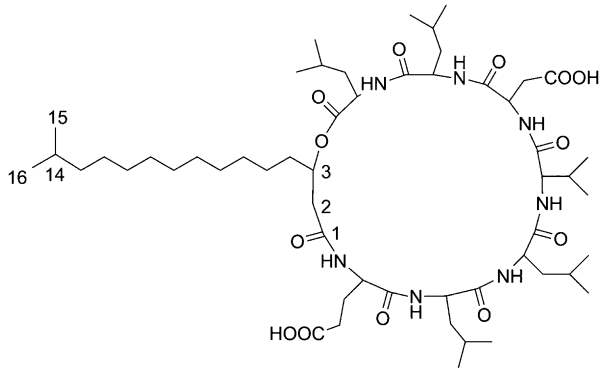

Figure 1. Chemical composition of un-ionized iso-C16 surfactin.

horse-saddle conformation proposed by Bonmatin et al.[3] Each of the simulated micelle consisted of 25 surfactin molecules. We built the initial configuration of the micelle according to the preassembled method of Tieleman et al.,[19] which was adopted by many micelle configuration studies.[11,18,26−28] The surfactin micelles were placed as follows: the input surfactin molecule was set to lie along the *x*-axis, with the carbon atom 14 (C14) on the origin and carbon atom 3 (C3) along the *x*-axis. The whole molecule was translated by 0.5 nm in the *x*-direction to avoid overlaps in the core of the micelle during the later rotation. Then the molecule was copied and rotated n_s (number of the surfactin molecules in each plane) times by $360/n_s$ degrees in the *xy*-plane. The procedure was repeated with five planes parallel to the *xy*-plane, with the molecule tails pointed toward the origin. The n_s of surfactin molecules in the five planes were 1, 7, 9, 7, and 1, respectively. Each micelle was placed in the center of a cubic box whose length is 10 nm; the box contained 31 757 SPC (simple point charge)[29] water molecules, and the water molecules were avoided being placed in the core of the micelles. Independent simulations were carried out at 277, 298, 323, and 343 K. The parameters of the force field of the surfactin were constructed by the PRODRG program.[30]

We used the GROMACS package (version 3.3)[31] and the GROMOS96 45a3 force field[32] for the MD simulations. The systems were energy minimized at first, and then a 20 ps position-restrained equilibration was performed. The systems were coupled to anisotropic pressure bath of 1 atm (τ_p = 1.0 ps), and a Berendsen thermostat was used to control the temperature.[33] All the bond lengths were constrained using LINCS,[34] and all the long-range electrostatic interactions were computed using the PME method[35] with a 1.0 nm cutoff range. The systems were then equilibrated for 5 ns with a time step of 2 fs, and the neighbor list was updated every 10 steps.

The equilibrium of the systems was detected by root-mean-square deviation from the mass center of the micelle ($RMSD_{mc}$). $RMSD_{mc}$ depicts the deviations of distances between atoms and the mass center of a micelle with respect to that of the micelle structure at the beginning with the expression as

$$\mathrm{RMSD_{mc}} = \left[\frac{1}{M}\sum_{i=1}^{N} m_i \| r_{ic}(t) - r_{ic}(0)\|^2\right]^{1/2} \quad (1)$$

where r_{ic} is the distance between atom *i* and the instantaneous center of mass (COM) of the micelle. When the fluctuations of $RMSD_{mc}$ are less than 1%, we regard the micelle system achieves equilibrium. The values of $RMSD_{mc}$ during the simulations at four temperatures are plotted in Figure 2. At

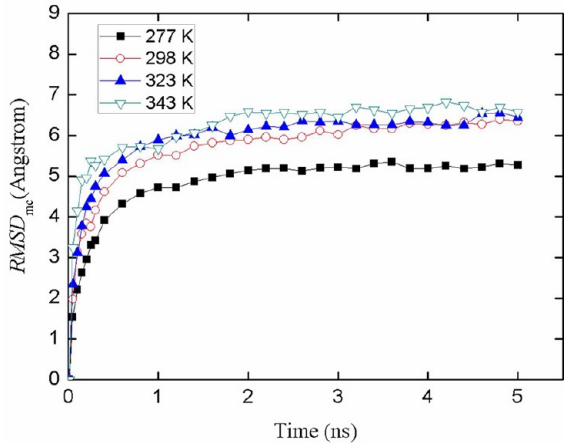

Figure 2. $RMSD_{mc}$ fluctuations of the surfactin micelles.

initial, the increment speed of the $RMSD_{mc}$ is more rapid at higher temperature as temperature accelerates the movement of the surfactin molecule and promotes the equilibrium of the micelles.

After equilibrium was achieved, MD trajectories were collected every 0.1 ps during the last 1 ns run for further analyses. In order to investigate the properties of hydrogen bonds, shorter simulations of 100 ps were run and during which atomic coordinates were saved every 20 fs.

3. RESULTS

3.1. Micelle Shape and Size. Principal moment of inertia (*I*) is a detailed analysis to depict the shape of a micelle.[14,19] I_{xx}, I_{yy}, and I_{zz} of each micelle are averages over the diagonalized inertia tensor at each time step. The principal moments of inertia of the micelles at four temperatures were collected in Table 1. The values of I_{xx}, I_{yy}, and I_{zz} of the micelles at each temperature are close to each other, which indicate that all the micelles are approximately in shapes of sphere. The asymmetry parameter, α, defined as $\alpha = (2I_{xx} - I_{yy} - I_{zz})/(I_{xx} + I_{yy} + I_{zz})$, could indicate the symmetry of a spherical shape. For a perfect sphere, the value of α would be zero. The asymmetry parameters of the micelles at four temperatures are around 0.1, which corresponds to a small degree of asymmetry from a spherical shape. The asymmetry parameters at different temperatures have little discrepancy from each other which indicate that the aggregate shape is not quite sensible to temperature.

One of the primary characteristics of micelle structure is its size. Given the assumption that the shapes of the micelles are mostly in sphere, we calculated the micelle radius to describe them. The radius of the micelle could be measured from the radius of gyration, R_g, over the course of the simulation. R_g is a measure of the distribution of the mass of atomic groups or molecules relative to the COM of the micelle, which could be expressed in the following expression:

$$R_g = \sqrt{\sum_i m_i (r_i - r_{com})^2 / \sum_i m_i} \quad (2)$$

where m_i is the mass of atom *i* located at a radial distance r_i from the COM of the aggregate core (r_{com}). The effective

dx.doi.org/10.1021/jp302413c | J. Phys. Chem. B 2012, 116, 12735−12743

Table 1. Principal Moments of Inertia[a] and Averaged Predicted Micellar Radius at Four Temperatures

T (K)	I_{xx}	I_{yy}	I_{zz}	α	R_s (nm)
277	5.82 ± 0.06	5.35 ± 0.07	4.46 ± 0.05	0.117	2.22 ± 0.01
298	5.36 ± 0.07	5.11 ± 0.07	4.42 ± 0.06	0.081	2.17 ± 0.01
323	5.53 ± 0.09	5.24 ± 0.08	4.38 ± 0.08	0.095	2.19 ± 0.01
343	5.39 ± 0.07	4.92 ± 0.13	4.42 ± 0.08	0.097	2.16 ± 0.01

[a]Moments of inertia in units of 10^4 amu nm^2.

Table 2. Solvent Accessible Surfaces Areas for the Total Micelle, the Hydrocarbon Chains from C4 to C16 (Tail), the Backbones of the Peptide Rings (Ring), the Lateral Chains in Hydrophilic Amino Acids (Hydrophilic aa), and the Lateral Chains in Hydrophobic Amino (Hydrophobic aa) on the Peptide Rings

SAS areas (nm^2)	277 K	298 K	323 K	343 K
total	112.7 ± 3.2	103.9 ± 1.3	104.8 ± 1.3	102.5 ± 1.8
tail	5.6 ± 0.5	5.8 ± 0.5	6.5 ± 0.7	18.9 ± 0.9
ring	17.5 ± 0.9	16.5 ± 0.6	16.5 ± 0.4	14.7 ± 0.7
hydrophobic aa	70.5 ± 3.6	68.6 ± 0.8	68.2 ± 1.3	58.3 ± 1.5
hydrophilic aa	18.9 ± 1.1	13.0 ± 0.5	13.7 ± 0.7	10.73 ± 0.6

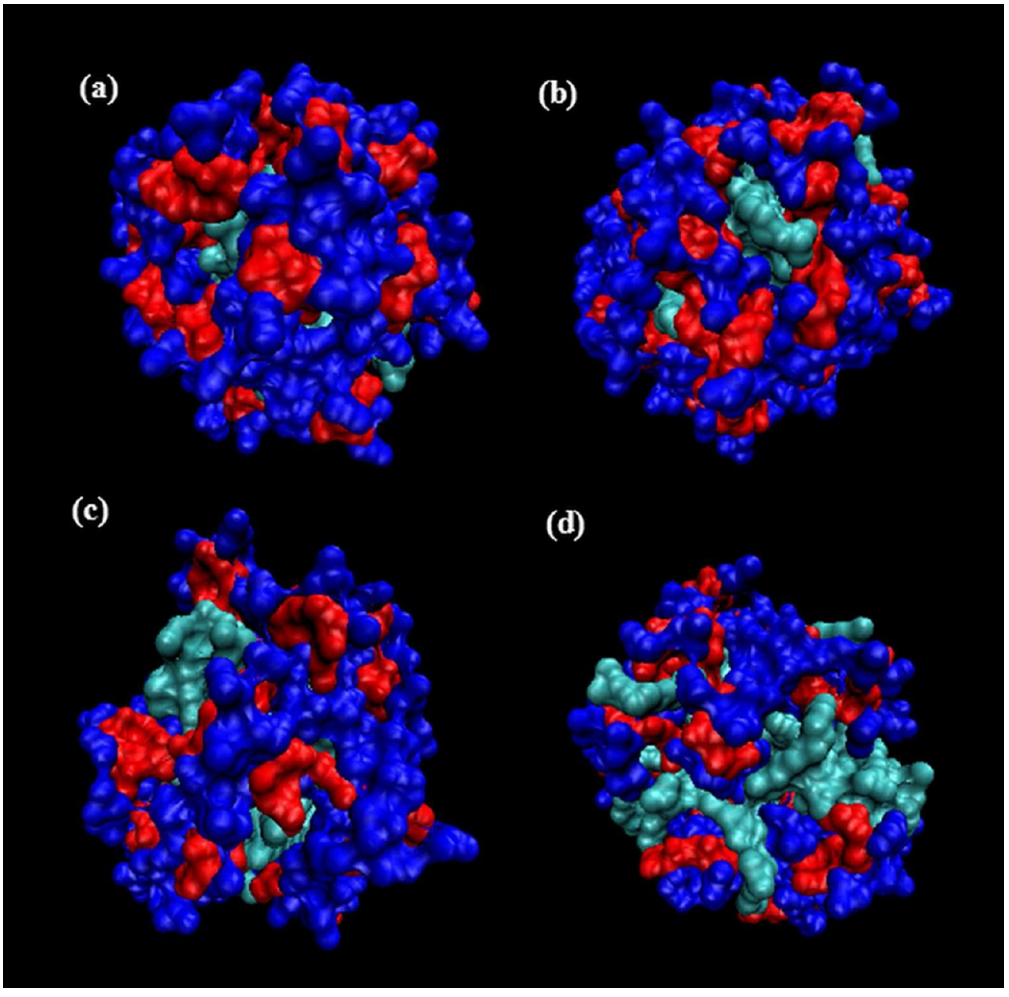

Figure 3. Pictorial view of equilibrated surfactin micelles at (a) 277, (b) 298, (c) 323, and (d) 343 K by VMD viewer.[38] The hydrocarbon chain was presented in cyan, the red color represents the backbone of the peptide ring, and the blue color represents the side chains of the amino acid residues.

micellar radius (R_s) was approximated by the following expression[36]

$$R_s = \left(\frac{5}{3}\right)^{0.5} R_g \quad (3)$$

which treats the micelles as spheres of uniform density. The average micellar radii were all around 2.2 nm (see Table 1). Besides, the micelle radii deduced at four temperatures have little discrepancy from the others, and we could infer that temperature would not greatly influence on the size of the micelles whose aggregate number is 25.

3.2. Micelle Interfacial Properties. Solvent accessible surface (SAS) area, a characteristic interfacial property which could quantitate hydrophobic burial extent, is the surface area of a biomolecule that is accessible to a solvent. Complete characterization of the interface between the micelle and the water is important as it is useful in understanding of how other hydrophilic species such as cells and membranes interact with their aqueous environment. The SAS areas of the surfactin micelles were calculated using Surface Racer 5.0[37] with a probe radius of 1.4 Å. In Table 2, we collected the SAS areas of several groups of the surfactin molecules in the micelles. Group tail represents the hydrocarbon chain from C4 to C16 which are labeled in Figure 1; group ring represents the backbone of the peptide ring; group hydrophilic aa is for lateral chains of the hydrophilic amino acids (Glu and Asp), and group hydrophobic aa is for lateral chains of hydrophobic amino acids (Leu and Val). The total SAS area gets a general decrease tendency with increasing temperature, though the aggregate size of surfactin micelle is temperature-independent. The majority of the contribution to the SAS of the micelle comes from the peptide rings (the headgroup of surfactin molecule), and more than 80% surface area between the micelle and water is contributed by the headgroup of the surfactin. The hydrocarbon chains (group tail) also have some expose areas on the micelle surface which contact with water.

When the temperature gets higher, the SAS area of group tail grows, whereas the SAS areas of hydrophilic aa and hydrophobic aa as well as of the group ring decline. Moreover, in order to give a direct visual inspection and comparison of the difference between the SAS areas of the micelle at different temperatures, Figure 3 presents the snapshots of surfactin micelle's surface structures drawn by VMD[38] at four temperatures. From the figure, it could be clearly seen that the peptide rings cover most of the surface of the sphere-shaped micelles and a few hydrocarbon chains exposed on the surface, and the exposure of the hydrocarbon chains enhances with the increasing temperature.

The interface between the surfactin micelles and the surrounding water could also be characterized by the radial distribution function (RDF) of oxygen and nitrogen atoms on the head groups with the oxygen atoms in water. Figure 4 presents the RDFs that characterize the oxygen atom−water (Ob-OW) and the nitrogen atom−water (N-OW) behavior (both Ob and N atoms are on the backbones of the peptide rings) as well as the free carboxyl oxygen atom−water (Oc-OW). There are not very sharp peaks in the three radial distribution functions. All the three figures show a similar tendency that the curve gets lower values with temperature increasing, demonstrating that higher temperature induces the loss of water molecules in the hydration shell of the micelle and a consequent dehydration.

3.3. Surfactin Orientation in Micelle. To estimate the effect of temperature on the spatial extent of the micelles, the mass density profiles, $\rho(r)$, of the water, the hydrocarbon chain (C4 to C16) groups, the peptide ring groups, the four leucine amino acid residues, and the other three amino acid residues in radial direction are depicted in Figure 5; r was the radial distance of each atom from the COM.

According to the density profiles, the hydrocarbon chains mainly distribute themselves within 1.5 nm from the COM along the radius direction. The peptide rings, the head groups of surfactins, have a broad distribution, and the shell of the peptide ring is from about 0.5 to 2.4 nm. The distribution of

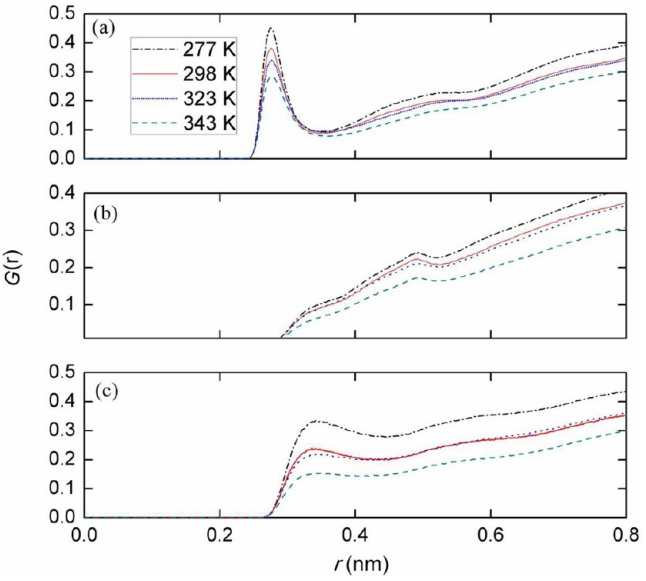

Figure 4. Radial distribution functions of surfactin micelle in water: (a) oxygen atom on the backbone of the peptide ring and water oxygen (Ob-OW); (b) nitrogen atom with water oxygen (N-OW); (c) oxygen atom in carboxyl groups with water oxygen (Oc-OW).

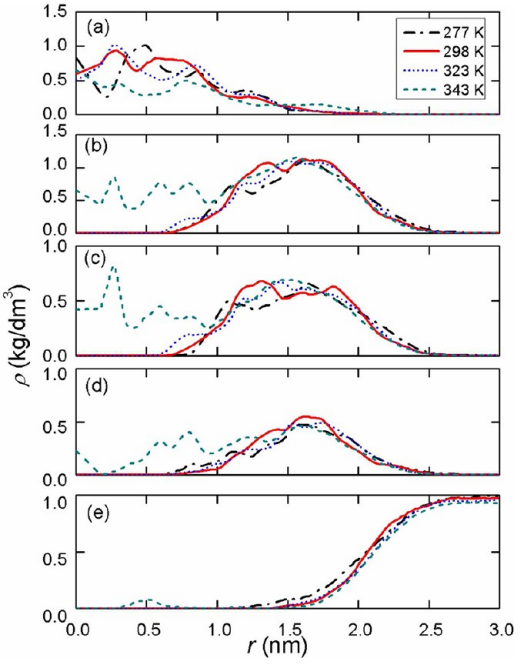

Figure 5. Radial densities of (a) the hydrocarbon chain, (b) the peptide ring, (c) the four leucines residues, (d) the other three amino acids residues (Glu, Asp, and Val), and (e) water.

peptide rings and the distribution of the hydrocarbon chains have an intersection with a slab of about 1.0 nm in the radius direction. At especially high temperature as 343 K, the profile of peptide ring has a much broader distribution and expands into the regions that originally occupied by the hydrocarbon chains. The range of the distributions of the four leucine amino acids and the peptide rings are identical, and they have a similar tendency as well.

From the profile of water in Figure 5e, we could observe that at higher temperature the profile of water retreats toward the positive direction of the r, resulting in the decrease of the

dx.doi.org/10.1021/jp302413c | J. Phys. Chem. B 2012, 116, 12735−12743

overlap of surfactin distribution and water distribution, and the water density at higher temperature is smaller than that at lower temperature from the region 1.5 to 2.3 nm, which proves the occurrence of dehydration that also obtained by the analysis of RDFs mentioned above. In the core of micelles, which consisted of the hydrocarbon chains, a slight water penetration is observed at 343 K. We consider that the surfactin micelle could be described as a two-shell model: the inner core shell that within a radius of 1.0 nm is mainly formed by the hydrocarbon chains; the outer shell mostly consisted of the peptide rings is from 1.0 to 2.0 nm, and the boundary between the surfactin micelle and the water is in the region from 2.0 to 2.5 nm along the radial direction.

To investigate the orientations of the peptide ring and the hydrocarbon chain of surfactin, we adopted three angles to examine the extent of torsional motions of the micelle. They are defined as follows: The angle alpha formed by the vector from C3 (β-carbon atom) to C14 (branched carbon in tail) and the vector from C3 to the COM of the micelle, the former vector could represent the orientation of the hydrocarbon chains and the latter one represents the radius direction of the micelle; the angle beta formed by the vector from C3 to COM and the vector from C3 to the COP (mass center of peptide ring), the vector from C3 to the COP could approximately represent the orientation of the plane of the peptide ring; and the angle gamma formed by the vector from C3 to C14 and the vector from C3 to COP. When the angle alpha is zero, the hydrocarbon chain is pointing directly at the COM of the micelle. And if alpha increases, the hydrocarbon chain deviates from the radial direction of the micelle. When the angle beta is 90°, it means that the peptide ring is in a tangent plane of the surface of the micelle sphere. When the angle gamma equals 90°, the hydrocarbon chain of the surfactin molecule is perpendicular to the plane of the peptide ring. We presented the illustration of the sites of COM and COP in Figure 6. Figure 7 shows the angular distributions of the three defined angles. Roughly, the alpha angles are mainly distributed around

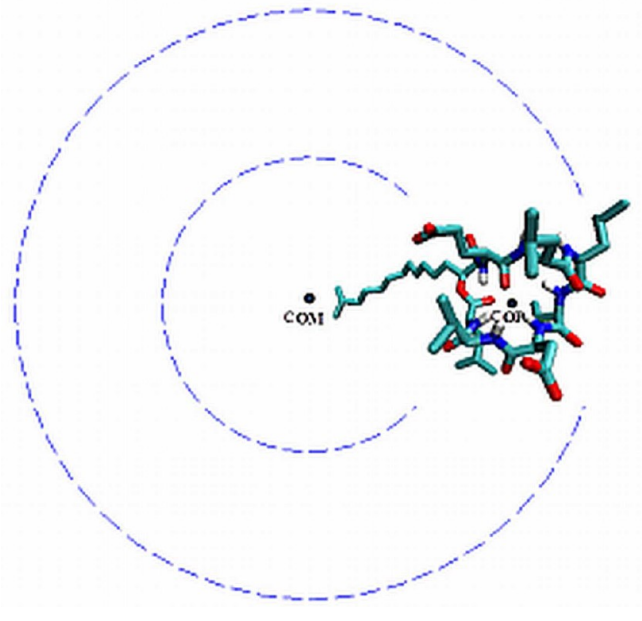

Figure 6. Illustration of the sites COM and COP involved in the three supposed angles.

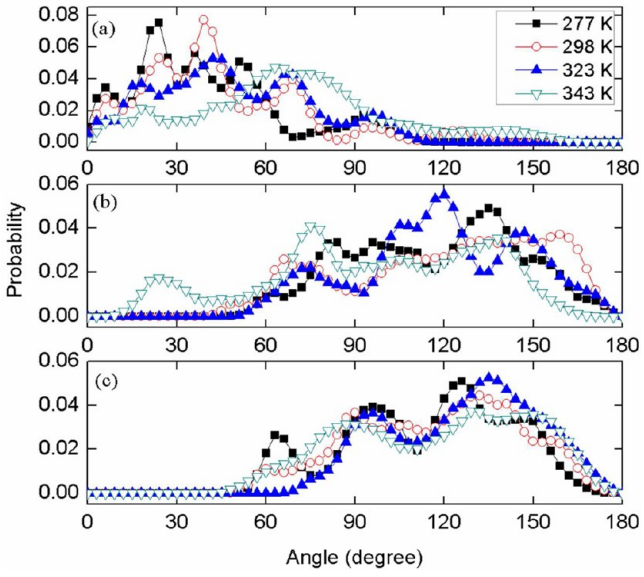

Figure 7. Angular distributions of (a) alpha, (b) beta, and (c) gamma. Alpha is the angle formed by the vector from C3 to C14 and the vector from C3 to the COM, beta is the angle formed between the vector from C3 to COM and the vector from C3 to the COP, and gamma is the angle formed between the vector from C3 to C14 and the vector from C3 to COP.

10°−100°. This indicates that the hydrocarbon chains of the surfactin monomers are not directly oriented toward the COM of micelle. They are not aligned the radial direction of the micelle as in the initial configuration of the system. When temperature gets higher, the alpha angle distribution shift to the positive direction which indicates that temperature would activate the movements of the surfactin molecules and more chains deviate from the radial direction of the micelle. And at 343 K, alpha angles exhibit bigger angular distribution that larger than 100°, indicating that some hydrocarbon chains changed their orientation and adopted a direction against the COM of micelle and thus expose to the micelle surface, which may be considered as "flip-flopped". These could be attributed to the violent movements of the monomers caused by higher temperature. From Figure 7b, the beta angle distributions occupy quite large ranges; the planes of the peptide rings are randomly placed in the micelle. Even though temperature still has some impact on the placement of the planes of the peptide ring, at 277 and 298 K, the curves are mainly distributed from 110° to 160°, which means the peptide rings did not spread themselves on the surface of the micelle and tended to erect themselves in order to keep their body away from the water. And when temperature rises to 343 K, less probability of the angles occurs at this region and the beta angles tend to be in range of 20°−40°. That means some peptide rings changed their orientation and faced to the COM of the micelle. At mean time, when temperature increases, the distribution of gamma angle, formed by C14, C3, and COP, slightly moves in the positive direction of the angle axis. The hydrocarbon chain tends to be in parallel with the plane of the peptide ring when temperature gets higher.

3.4. Surfactin Conformation in Micelle. In order to investigate the influence of the temperature on the conformation of the peptide ring, the average root-mean-square deviation (RMSD) of the peptide ring from its original horse-saddle conformation was estimated. Besides, we also calculated

dx.doi.org/10.1021/jp302413c | J. Phys. Chem. B 2012, 116, 12735−12743

the distances of two vectors as **CC** and **NN**.[24] Distance between vector **CC** connecting the C3 of the fatty acid and the α-carbon atom in chain 4 (Val), which represents the two top points of the hydrophobic side of the horse-saddle conformation. Vector **NN**, which connects the nitrogen atom of chain 2 (Leu) and the nitrogen atom of chain 6 (Leu), corresponds to the two top points of the hydrophobic side of the horse-saddle conformation. In Table 3, we collected the

Table 3. Average Lengths of CC and NN Vectors and RMSD of the Backbone of the Peptide Ring at Four Temperatures

T (K)	|CC| (Å)	|NN| (Å)	RMSD (Å)
original	4.6	5.5	
277	7.3 ± 1.6	6.1 ± 1.1	1.9 ± 0.3
298	7.6 ± 1.3	6.9 ± 1.1	2.0 ± 0.3
323	8.0 ± 1.5	6.6 ± 1.5	2.1 ± 0.3
343	8.5 ± 1.5	6.1 ± 1.3	2.2 ± 0.3

data of the lengths of **CC** and **NN** and the RMSD values of the backbones of peptide rings derived from the four temperatures. The length of **CC** vector increases, while the length of **NN** vector has a reverse variation with the increasing temperature. It seems that the peptide ring tends to turn into looplike conformations at higher temperature compared with the original horse-saddle structure. The value of RMSD increases as the conformations of the peptide rings deviate more from the original ones at higher temperature.

The dihedral angle, α_{dih}, was introduced in order to characterize whether the surfactin molecules adopt the horse-saddle shape in micelle. It corresponds to the dihedral angle between plane α-CH(4)−NH(2)−CO(5) and plane NH(2)−CO(5)−C3, which is illustrated in Figure 8a. The horse-saddle

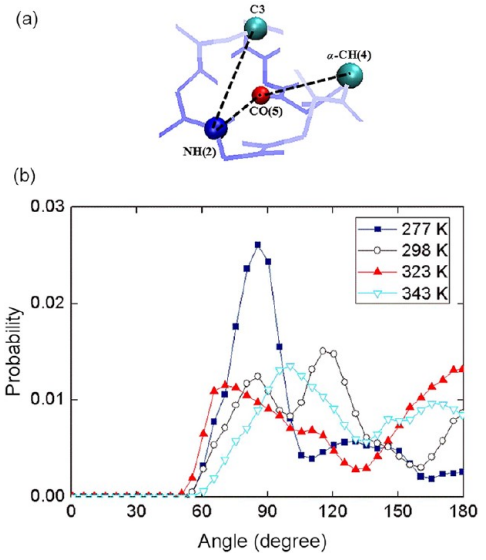

Figure 8. (a) Illustration of the tetrahedron angle. (b) Tetrahedron angle distributions at four temperatures.

conformation has a value of 65.57° for α_{dih}, and a value close to 180° corresponds to a flat peptide ring structure. Figure 8b displays the probabilities of the dihedral angle, α_{dih}, of the surfactin molecules in the micelle. At 277 K, α_{dih} angle is mainly in the range of 60°−100°; when the temperature increases, the distribution shifts to the positive direction of angle axis, illustrating that peptide rings tend to open up their horse-saddle structure at higher temperature. According to the angular distribution of α_{dih} that exceed 140° at temperature of 323 and 343 K, nearly 30% of the peptide rings become flat planes.

We also calculated the gauche defect probability,[13] which is defined as the probability of the kink in sequence *i-j-k-l*, whose dihedral angle between the planes *i-j-k* and *j-k-l* is between 30° and 110°. The values of the gauche defect probability of the hydrocarbon chains are in a range of 0.2−0.3, and the temperature has little impact on gauche defect probability. It can be inferred that the tails are quite flexible because the gauche defect probability for the surfactin molecule in the micelle is higher than that of SDS molecule (around 0.15) in the micelle,[13] which has similar micellar size of the simulated surfactin micelle.

3.5. Hydrogen Bond Dynamics in Micelle. Because the amino acid residues of the surfactin could easily approach others in a micelle, it would be quite interesting to observe whether temperature would impact the interactions between surfactin molecules. We detected both intra-hydrogen bonds formed in a surfactin molecule and inter-hydrogen bonds formed between surfactin molecules. The geometrical criterion of the formation of hydrogen bonds is at a cutoff distance of 4 Å between the D (hydrogen donor) and A (hydrogen acceptor), and a minimum angle of 120° for D−H···A according to the generous criterion for the hydrogen bonds formed between peptides that used by Kieseritzky et al.[39]

The stability of the hydrogen bonds is evaluated by a time correlation function (TCF), namely, the continuous hydrogen bond time correlation function, $S_{HB}(t)$. $S_{HB}(t)$ describes the probability that a hydrogen bond formed between two sites at time zero and continually bonded up to time t which is in the form of

$$S_{HB}(t) = \frac{\langle h(0)H(t)\rangle}{\langle h(0)h(0)\rangle} \quad (4)$$

where $\langle\cdots\rangle$ means the calculation is carried out by averaging the hydrogen bonds that formed at different time origins. $h(t)$ takes the value 1 if the hydrogen bond is present at time t and the value of 0 otherwise, and $H(t)$ is unity when the monitored pair of sites continuously hydrogen bonded in an interval of 0−t and zero otherwise. Therefore, $S_{HB}(t)$ could explore the direct lifetime of the hydrogen bonds in the micelles. The mean relaxation time or the hydrogen bond lifetime $\langle\tau\rangle$ is the integral of the correlation function $S_{HB}(t)$.

The continuous TCF are separately calculated for the hydrogen bonds formed inside a peptide ring (SI) and that between peptide rings (SS), and Figure 9 displays the curves of the relaxation of the continuous time correlation function, $S_{HB}(t)$, for SI and SS hydrogen bonds. It can be clearly observed from Figure 9 that all the correlation functions decayed rapidly. The parameters of the fit of exponential functions to the TCFs are provided in Table 4. The exponential fitting parameters to the TCFs are provided according to a multiexponential equation, $y = A_1 \exp(-t/\tau_1) + A_2 \exp(-t/\tau_2)$. The lifetime of SI and SS hydrogen bonds, τ_{SI} and τ_{SS}, are calculated as the integral of the correlation functions, $S_{HB}^{SI}(t)$ and $S_{HB}^{SS}(t)$.

The lifetimes of SS and SI hydrogen bonds in the surfactin micelle are quite short. Besides, the lifetimes of both SI and SS hydrogen bonds decrease with temperature increasing, which

dx.doi.org/10.1021/jp302413c | J. Phys. Chem. B 2012, 116, 12735−12743

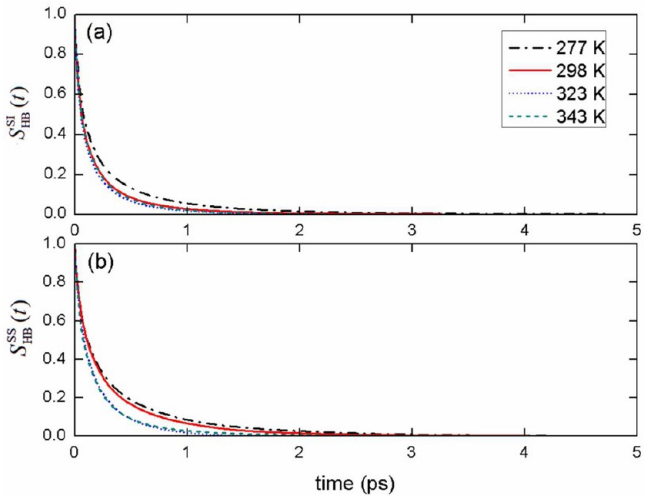

Figure 9. Continuous hydrogen bond time correlation function, $S_{HB}(t)$, of (a) SI hydrogen bonds, $S_{HB}^{SI}(t)$, and (b) SS hydrogen bonds, $S_{HB}^{SS}(t)$.

also illustrates that the motional activity of the molecules is enhanced at higher temperature and induces the instability of the hydrogen bonds.

We have recorded the possible β-turn and γ-turn conformations in the peptide ring by counting the hydrogen bonds occurring at specific sites. The peptide rings could form β-turn conformations through the occurrence of the hydrogen bonds at NH(5)−CO(2) and CO(5)−NH(2); they could form γ-turn conformations through the occurrence of the hydrogen bonds at NH(4)−CO(2), NH(7)−CO(5), and NH(6)−C^{1}O. The possibilities of the hydrogen bonds at these sites were all calculated. We found that the probabilities of the hydrogen bonds formed at these sites are as low as 1%. The mostly occurred hydrogen bonds maintaining β−turn conformations are at the site NH(5)−CO(2) and those maintaining γ-turn conformations are at the sites of NH(4)−CO(2) and NH(7)−CO(5). The hydrogen bonds at site NH(6)−C^{1}O almost never happen. In addition, the occurrence possibility of hydrogen bonds at site NH(7)−CO(5) decreases with the increasing temperature.

The Ramachandran angles at these sites were also calculated in order to determine the types of these turn structures. According to the Ramachandran angles of these sites, the surfactin molecules mostly adopt type IV β-turn and inverse type γ-turns. Besides, the fractions of type II β-turn at site NH(5)−CO(2) and classic type γ-turn at site NH(7)−CO(5) decrease when temperature increases. The possibilities of different types of the turn structures are recorded in Table 5.

Table 5. Percentages of Types of the Turns at Specific Positions of β-Turns and γ-Turns

	β-turn				γ-turn			
	NH(5)−CO(2)		CO(5)−NH(2)		NH(4)−CO(2)		NH(7)−CO(5)	
T (K)	II	IV	II	IV	classic	inverse	classic	inverse
277	4.5	95.5	14.6	85.4	25.0	72.1	22.3	76.9
298	0.7	99.3			0	98.4	25.6	73.9
323	0.2	99.8	3.8	96.2	31.3	66.2	7.0	92.3
343	0.1	99.9	6.8	93.2	0.1	99.2	0.3	98.5

Besides, we presented the Ramachandran plots (Φ_{i+1}, Ψ_{i+1}) and (Φ_{i+2}, Ψ_{i+2}) of the β-turn at site NH(5)−CO(2) and the Ramachandran plots (Φ_{i+1}, Ψ_{i+1}) of the γ-turn at site NH(4)−CO(2) and NH(7)−CO(5) in Figure S1 and Figure S2, respectively, in the Supporting Information. There exists two regions in all the plots in Ramachandran plots of the two sites of γ-turns, which represent inverse type (the left region) and classic type (the right region), respectively.

4. DISCUSSION

The surfactin micelles in our simulation are mostly in spherical shape with very low asymmetry values. The micelles are ∼2.2 nm in radius, which is in accordance with the result of 50 ± 5 Å in diameter obtained by the SANS experiment at 298 K.[10] The radius derived from the diffusion coefficient given by DLS gave a much larger radius of 4−6 nm[9] because the radius obtained from the diffusion coefficients will include bound water; this would cause uncertainty in the determination of the micelle radius and may overcharacterize the size. Besides, the change of the radius of the surfactin micelle detected in our simulation is not very sensitive to temperature. We also noticed that the distributions of the four leucine amino acids and those of the peptide rings are almost in the same region along the radius direction, and they have similar tendency profiles of the curves as well. It seems that the leucine amino acids were normally distributed in the shell consisted of the peptide rings, which is not in accordance with the model assumed by Shen et al.[10] that the core contains all of the chain group and the four leucines. As a study[40] shows that the decrease of pH neutralizes the COO^- groups in the glutamic and aspartic amino acid residues, which will induce conformational changes of surfactin molecules which lead to different aggregation. As the un-ionized surfactin micelles have not been studied by experiments so far, the study of the un-ionized surfactin micelles would be a reference to the studies of the ionized surfactin micelles.

SAS gives a profile description of the interfacial property between the surface of the micelle and the surrounding water.

Table 4. Exponential Fitting Parameters to the Continuous TCFs of SI and SS hydrogen bonds

		intramolecular (SI)				intermolecular (SS)		
T (K)		time constant (ps)	amplitude (%)	$\langle\tau_{SI}\rangle$ (ps)		time constant (ps)	amplitude (%)	$\langle\tau_{SS}\rangle$ (ps)
277	τ_1	0.08	61	0.24	τ_1	0.10	56	0.32
	τ_2	0.58	33		τ_2	0.69	39	
298	τ_1	0.38	36	0.17	τ_1	0.09	54	0.28
	τ_2	0.06	61		τ_2	0.55	42	
323	τ_1	0.06	39	0.14	τ_1	0.28	54	0.18
	τ_2	0.30	59		τ_2	0.05	45	
343	τ_1	0.05	58	0.16	τ_1	0.28	54	0.18
	τ_2	0.32	40		τ_2	0.05	45	

dx.doi.org/10.1021/jp302413c | J. Phys. Chem. B 2012, 116, 12735−12743

The majority of the contribution to the SAS of the surfactin micelle comes from the peptide rings. More than half of the area of the peptide ring concentrates on the side chains of the amino acids; the atoms on the side chains of amino acids, which own the most quantity of the atoms of the peptide ring, could contact more water than the backbone of the peptide ring on the micelle surface. We estimate that the side chains of the amino acids occupy the outer shell of the micelles and shield the water from the interior of the micelle as much as possible. Besides, the hydrocarbon chains have some exposed areas on the micellar surface because the headgroup is a hollow ring and could not completely cover the surface of the micelle; there exists some cavities allowing the penetration of water into the micelle cores, thus providing chances for water molecules to contact with the hydrocarbon chains of surfactin molecules. The distribution of the hydrocarbon tails in Figure 3 could also prove this fact. When the temperature gets higher, the total SAS area of surfactin micelle and the SAS area of peptide ring group decreased; in other words, the surfactin micelle reduced the interfacial contact area, mainly of the peptide ring group, with the surrounding water. This could be due to the temperature dehydration as the higher temperature induces the outside shell of the micelle to lose water molecules. The trend of the changes in RDF profiles also demonstrates that temperature dehydration occurs. These behaviors obey the general rule for almost all surfactants as the hydration degree of micelles decreases upon the increasing temperature. The polar interaction between surfactin micelle and water molecule decreased as more hydrocarbon chains exposed to the aqueous solution, and thus water molecules moved away more easily from micellar surface at higher temperature. Thus, when the temperature increases, the backbone of the peptide ring, the side chains of both the hydrophobic amino acids and the hydrophilic amino acids all have a tendency to reduce the SAS area contacting with water. Interestingly, at 343 K, there exists a larger increase of the exposed area of the chain tails to water. That is due to the fact that some surfactin molecules reversed themselves and orient their chain tails to the surface of the micelles as flip-flopped, which can be evaluated by the angular distribution of alpha and beta mentioned above. We assume that higher temperature induced violent movements of the molecules and increased the probability of this kind of molecule reversal. At mean time, some water molecules penetrate into the inner core of micelle (see Figure 5e).

The hydrogen bonds of NH(5)−CO(2)/CO(5)−NH(2) and NH(4)−CO(2)/NH(7)−CO(5), which respectively characterized the β-turn and γ-turn structure of the peptide ring, could be detected in the simulation. Besides, circular dichroism spectra measurements also detected that the peptide rings adopt the β-turn conformations at relatively low concentration.[9] Though the structures of turns are very essential in the folding of proteins, especially in cyclic peptides,[25] the low occurrence probabilities (around 1%) obtained in the present simulation imply that these structures rarely occurred in surfactin micelles in water solution. Unlike other folded peptides, the peptide rings of the surfactin molecules contact mostly with the surrounding water and the rapid movement of the water molecules would easily strike on the atoms which maintain β-turn or γ-turn structure, it is quite difficult for the peptide rings to maintain the second structure as turns in solution. These turn conformations also had very short lifetimes due to the large distances between atoms caused by the structural expansion of the peptide ring backbone when the surfactin molecules were at the hydrophilic/hydrophobic interfaces.[22,24] Types of the turn conformations characterized by Ramachandran angles have been influenced by the increasing temperature to a certain extent (can be seen in the Supporting Information) as the portion of type IV β-turn and type inverse γ-turn decrease with temperature increasing. That is somehow related with that the peptide rings gradually turn into a looplike conformations as the length of **CC** vector increases upon the increasing temperature (Table 3), and the tetrahedron angles of the peptide ring are close to 180°. At meantime, intramolecular hydrogen bonds (SI) have very short lifetimes. It is due to the fact that the structural expansion of the peptide ring backbone occurred, the spatial distances between the atoms that could form hydrogen bonds increased, and it would reduce the probability of the interaction of these atoms. Intramolecular hydrogen bonds in the surfactins are influenced by the temperature, where lifetimes of the SI hydrogen bonds decrease with temperature increasing. As the increasing temperature induces the increasing movements of the surfactin molecules, which would be easily illustrated by RMSD for peptide ring backbones, thus leads to the easy breakage of hydrogen bonds formed in the peptide rings. The intermolecular hydrogen bonds (SS) also have very short lifetimes and they are affected by the change of temperature as well. It was assumed that larger surfactin aggregates may be the aggregates of small micelles by intermicelle hydrgen bonds.[9] We infer that small surfactin aggregates would be harder to aggegate into larger micelles at higher temperature and the hydrogen bond interaction in the micelles might not be the dominant reason to maintain the micelle structure.

5. CONCLUSIONS

In this paper, we have performed molecular dynamic simulations of surfactin micelles at four temperatures in aqueous solution. We focused on obtaining more insight into the structure and the interfacial properties of the micelles at a molecular level and their dependence on the temperature. The surfactin micelles are roughly spheres in our simulations with estimated radii around 2.2 nm. The temperature has impacts on the structures of the micelles exhibiting the surface shrinks of the sphere structure and the increased expose of the hydrocarbon chains with the increasing temperature. It is also observed that the hydration degree of the micelles decreases upon the increasing temperature, and the water shell weakens due to the temperature dehydration. The increasing temperature also damages the stability of the hydrogen bonds in the micelles. The secondary structures of the peptide rings such as β-turn and γ-turn in a rare low probability have been detected in surfactin micelle. The peptide rings seldom adopt horse-saddle conformations and tend to be in flat structures when temperature increases.

The results obtained here demonstrate that the temperature would have an important influence on the inner structure of the surfactin micelles. We believe that our micelle model is useful as a basic model for realistic micellar structure of surfactin micelles. Although we have studied the interface of the micelles, the interactions between the surfactin and the hydration water around the micelles have not been studied yet, and our investigations in this part are now in progress.

■ ASSOCIATED CONTENT

Supporting Information

Additional Ramachandran plots of β-turn and γ-turns at special sites of the peptide ring (Figures S1 and S2); the force field parameters of the surfactin molecule (Table S1). This material is available free of charge via the Internet at http://pubs.acs.org.

■ AUTHOR INFORMATION

Corresponding Author

*Tel +86-21-64252063; Fax +86-21-64252458; e-mail bzmu@ecust.edu.cn.

Notes

The authors declare no competing financial interest.

■ ACKNOWLEDGMENTS

This work was supported by the National Natural Science Foundation of China (Grant No. 21203063).

■ REFERENCES

(1) Arima, K.; Kakinuma, A.; Tamura, G. *Biochem. Biophys. Res. Commun.* **1968**, *31*, 488−494.
(2) Nagai, S.; Okimura, N.; Ohki, K.; Kanotomo, S. *Chem. Pharm. Bull.* **1996**, *44*, 5−10.
(3) Bonmatin, J. M.; Genest, M.; Labbe, H.; Ptak, M. *Biopolymers* **1994**, *34*, 975−986.
(4) Gallet, X.; Deleu, M.; Razafindralambo, H.; Jacques, P.; Thonart, P.; Paquo, M.; Brasseur, R. *Langmuir* **1999**, *15*, 2409−2413.
(5) Vollenbroich, D.; Ozel, M.; Vater, J.; Kamp, R. M.; Pauli, G. *Biologicals* **1997**, *25*, 289−297.
(6) Weislow, O. S.; Kiser, R.; Fine, D. L.; Bader, J.; Shoemaker, R. H.; Boyd, M. R. *J. Natl. Cancer Inst.* **1989**, *81*, 577−586.
(7) Kameda, Y.; Ouhira, S.; Matsui, K.; Kanatomo, S.; Hase, T.; Atsusaka, T. *Chem. Pharm. Bull.* **1974**, *22*, 938−944.
(8) Knoblich, M.; Matsumoto, R.; Ishiguro, K.; Murata, Y.; Fujiyoshi, Y.; Ishigami, M. O. *Colloids Surf., B* **1995**, *5*, 43−48.
(9) Han, Y.; Huang, X.; Cao, M.; Wang, Y. *J. Phys. Chem. B* **2008**, *112*, 15195−15201.
(10) Shen, H. H.; Thomas, R. K.; Chen, C. Y.; Daton, R. C.; Baker, S. C.; Penfold, J. *Langmuir* **2009**, *25*, 4211−4218.
(11) Bruce, C. D.; Berkowitz, M. L.; Perera, L.; Forbes, M. D. E. *J. Phys. Chem. B* **2002**, *106*, 3788−3793.
(12) Bruce, C. D.; Senapati, S.; Berkowitz, M. L.; Perera, L.; Forbes, M. D. E. *J. Phys. Chem. B* **2002**, *106*, 10902−10907.
(13) Sammalkorpi, M.; Karttunen, M.; Haataja, M. *J. Phys. Chem. B* **2007**, *111*, 11722−11733.
(14) Jalili, S.; Akhavan, M. *Colloids Surf., A* **2009**, *352*, 99−102.
(15) Palazzesi, F.; Calvaresi, M.; Zerbetto, F. *Soft Matter* **2011**, *7*, 9148−9156.
(16) Poghosyan, A. H.; Arsenyan, L. H.; Gharabekyan, H. H.; Falkenhagen, S.; Koetz, J.; Shahinyan, A. A. *J. Colloid Interface Sci.* **2011**, *358*, 175−181.
(17) Chong, T. T.; Hashim, R.; Bryce, R. A. *J. Phys. Chem. B* **2006**, *110*, 4978−4984.
(18) Abel, S.; Dupradeau, F. Y.; Raman, E. P.; Mackerell, A. D.; Marchi, M. *J. Phys. Chem. B* **2011**, *115*, 487−499.
(19) Tieleman, D. P.; van der Spoel, D.; Berendsen, H. J. C. *J. Phys. Chem. B* **2000**, *104*, 6380−6388.
(20) Marrink, S. J.; Tieleman, D. P.; Mark, A. E. *J. Phys. Chem. B* **2000**, *104*, 12165−12173.
(21) Lazaridis, T.; Malik, B.; Chen, Y. *J. Phys. Chem. B* **2005**, *109*, 15098−15106.
(22) Nicolas, J. P. *Biophys. J.* **2003**, *85*, 1377−1391.
(23) Gang, H. Z.; Liu, J. F.; Mu, B. Z. *J. Phys. Chem. B* **2010**, *114*, 14947−14954.
(24) Gang, H. Z.; Liu, J. F.; Mu, B. Z. *J. Phys. Chem. B* **2010**, *114*, 2728−2737.
(25) Gang, H. Z.; Liu, J. F.; Mu, B. Z. *J. Phys. Chem. B* **2011**, *115*, 12770−12777.
(26) Sterpone, F.; Marchetti, G.; Pierleoni, C.; Marchi, M. *J. Phys. Chem. B* **2006**, *110*, 11504−11510.
(27) Wang, Z. W.; Larson, R. G. *J. Phys. Chem. B* **2009**, *113*, 13697−13710.
(28) Yakovlev, D. S.; Boek, E. S. *Langmuir* **2007**, *23*, 6588−6597.
(29) Berendsen, H. J. C.; Postma, J. P. M.; van Gunsteren, W. F.; Hermans, J. *Intermolecular Forces*; Reidel: Dordrecht, 1981.
(30) Schuettelkopf, A. W.; van Aalten, D. M. F. *Acta Crystallogr., Sect. D: Biol. Crystallogr.* **2004**, *60*, 1355−1363.
(31) Lindahl, E.; Hess, B.; van der Spoel, D. *J. Mol. Model.* **2001**, *7*, 306−317.
(32) Schuler, L. D.; Daura, X.; van Gunsteren, W. F. *J. Comput. Chem.* **2001**, *22*, 1205−1218.
(33) Berendsen, H. J. C.; Postma, J. P. M.; Van Gunsteren, W. F.; DiNola, A.; Haak, J. R. *J. Chem. Phys.* **1984**, *81*, 3684−3690.
(34) Hess, B.; Bekker, H.; Berendsen, H. J. C.; Fraaije, J. G. E. M. *J. Comput. Chem.* **1997**, *18*, 1463−1472.
(35) Essman, U.; Perela, L.; Berkowitz, M. L.; Darden, T.; Lee, H.; Pedersen, L. G. *J. Comput. Chem.* **1995**, *103*, 8577−8593.
(36) Bogusz, S.; Venable, R. M.; Pastor, R. W. *J. Phys. Chem. B* **2000**, *104*, 5462−5470.
(37) Tsodikov, O.; Record, T.; Sergeev, Y. *J. Comput. Chem.* **2002**, *23*, 600−609.
(38) Humphrey, W.; Dalke, A.; Schulten, K. *J. Mol. Graphics* **996**, *14*, 33−38.
(39) Kieseritzky, G.; Morra, G.; Knapp, E. W. *J. Biol. Inorg. Chem.* **2006**, *11*, 26−40.
(40) Shen, H. H.; Lin, T. W.; Thomas, R. K.; Taylor, D. J. F.; Penfold, J. *J. Phys. Chem. B* **2011**, *115*, 4427−4435.